



Enhancing Ductile-mode Cutting of Calcium Fluoride Single Crystals with Solidified Coating

Yan Jin Lee¹ · Jing Yi Chong¹ · Akshay Chaudhari¹ · Hao Wang¹

Received: 10 January 2019 / Revised: 7 May 2019 / Accepted: 23 May 2019 / Published online: 19 June 2019
© Korean Society for Precision Engineering 2019

Abstract

Positive improvements have been observed during machining brittle materials under high hydrostatic pressure, but the techniques to achieve such desirable effects often utilize complex and expensive equipment or tools. This work presents a cost-efficient method to achieve ductile-mode machining of brittle materials at higher uncut chip thicknesses, by the application of a solidified coating on workpiece surface before a machining process. Orthogonal microcutting experiments were conducted on calcium fluoride single crystals oriented with the (111) plane and an increase in critical uncut chip thickness was observed with the solidified coating. The primary cause has been resolved to be mechanical-related and results in a stabilized microcutting process. Transmission electron microscopy provided evidence of slip deformation occurring in the machined subsurface regions and a layer thickness of subsurface damages reduced by ~45% under the influence of the solidified coating. In addition, erratic fluctuations in direction of the resultant machining force were subdued with the applied coating, which is proved to be caused by the compressive stresses induced from the sandwiching of the CaF₂ material between the tool and the solidified coating. The proposed technique successfully reduces the cost and pollution in the fabrication process of optical components from the use of coolant in an ultraprecision machining process to the time consumed by eliminating the subsurface damage with abrasive slurries in post-machining polishing.

Keywords Calcium fluoride · Ductile-mode cutting · Microcutting · Surface integrity · Ultraprecision machining

List of Symbols

r	Tool nose radius
w	Width of groove
a_p	Uncut chip thickness
F_c	Cutting force
F_t	Thrust force
F_R	Resultant force
F_s	Shear force
ζ	Resultant force inclination angle

1 Introduction

Over the recent years, the development of materials in the semiconductor and optics industries is extremely popular in view of the exclusive electronic and physical

properties. Calcium fluoride (CaF₂) is commonly used in advanced optical systems due to its wide transmission range (0.125–12 μm) and chemical stability [1]. However, this material presents a great tendency to exhibit brittle failure through the formation of microcracks on the machined surface. With the aid of an ultraprecision machining center equipped with single crystal diamond cutting tool, ductile-mode machining can be realized with a deterministic uncut chip thickness to produce crack-free freeform surfaces on semiconductors and optical components [2, 3]. Prior to brittle failure, ductile-regime cutting manifests when machining below a material specific critical uncut chip thickness, further known as the ductile–brittle transition (DBT), and removes work material by plastic flow [4]. Nakasuji et al. [5] proposed two mechanisms for the DBT to occur: (1) plastic deformation by slip along the characteristic slip plane and cleavage fracture relative to the cleavage plane, and (2) the density of subsurface defects encompassed by critical stress field ahead of the cutting tool that influences the critical stress values for slip and cleavage. Hence, the DBT is unique to each material and crystallographic orientation. Under ductile-mode cutting conditions, the workpiece material is

✉ Hao Wang
mpewhao@nus.edu.sg

¹ Department of Mechanical Engineering, Faculty of Engineering, National University of Singapore, 9 Engineering Drive 1, Singapore 117575, Singapore

deformed plastically, and continuous chips can be produced. The primary slip system and cleavage plane of CaF_2 crystal is $\{001\}\langle\bar{1}\bar{1}0\rangle$ and (111) , respectively.

A substantial body of research has been invested to develop unique ultraprecision machining techniques to enhance the machinability of brittle materials (i.e. increasing the critical uncut chip thickness to achieve crack-free surface finishing). Suzuki et al. [6] performed ultrasonic elliptical vibration cutting to significantly increase the critical undeformed chip thickness of sintered tungsten carbide, zirconia ceramics, calcium fluoride and glass. To et al. [7] showed an improvement in critical uncut chip thickness of hydrogen ion implanted silicon on an ultraprecision raster milling machine. Thermally enhanced microcutting was also proposed to activate secondary slip systems [8, 9] and reduce the material yield strength for increased plasticity during machining [10]. Ductile-mode machining of brittle materials was also observed at depths beyond the respective critical values inside a constructed pressurized steel vessel that induced an external hydrostatic pressure [11, 12].

1.1 Hydrostatic Pressure on Brittle Materials

The first observation on the enhanced ductility of brittle materials was made by Bridgman [13] in 1947. Compression and tensile tests under an external hydrostatic pressure by complete liquid immersion were performed on several materials such as glass (Pyrex) and synthetic sapphire (Al_2O_3). It was believed that the externally applied pressure influenced the net stresses acting on the material required for an energy-releasing process that determined the corresponding fracture strength of the material.

Two energy-releasing processes occur under tensile force conditions. Namely, the work done in elongation from the tensile forces and the work done by the liquid pressure acting on cracks formed on the external surfaces as shown in Fig. 1a. Furthermore, the increase in lateral contraction with increase in tension forces displaces molecules which serve as internal wedges for fracture initiation during tension. On the other hand, the increase in material volume upon release of compressive forces during compression testing produces the only energy-releasing process for failure, while work is done against the external pressure as shown in Fig. 1b. Therefore, higher compressive stresses on the brittle materials could be observed before failure, under the externally applied pressure.

1.2 Machining of Brittle Materials under Hydrostatic Pressures

The study of machining under an externally applied hydrostatic pressure was inspired by the positive enhancements in machining brittle materials with large negative

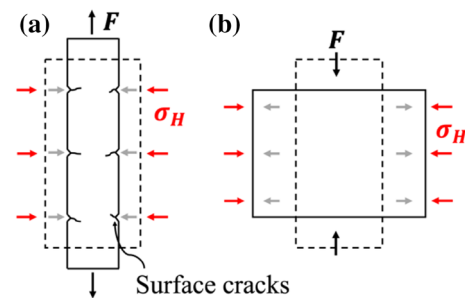


Fig. 1 Schematic of fracture processes under externally applied hydrostatic pressures in: (a) tensile and (b) compressive tests

rake angled cutting tools. The improvement follows the increase in hydrostatic pressure beneath the cutting tool that increases the material plasticity for ductile-regime machining. This has been proven to be true across all scales of brittle material machining, from macroscale drilling of rocks [14] to nanometric grinding process [15].

Yoshino et al. [16] developed a machining apparatus and performed constant-load scratching of silicon in vessel pressurized to 400 MPa with kerosene. Multiple cracks were observed under normal conditions, but smooth surfaces were produced on the grooves under the applied hydrostatic pressure. Yan et al. [12] used the same device to perform facing experiments on single crystal silicon using a single crystal diamond tool. Smooth crack-free surfaces were reported when machining under external hydrostatic pressure, with the generation of continuous chips similar to that observed in machining ductile metals. Yoshino et al. [17] later developed a new apparatus to study the effects of the externally applied hydrostatic pressure on various glassy materials, and crystalline structured brittle materials. They reported greater influences of the hydrostatic pressure on crystalline materials, with an increase in the DBT by an order of six and nine for silicon and quartz, respectively.

One school of thought for the increase in ductility is the structural transformation into a metallic state in the workpiece material under high hydrostatic pressure [12]. Another generic theory for the mechanism for improvement in machinability of brittle materials can be described as the suppression of subsurface micro-crack propagation. Yoshino et al. [11] reasoned that the existence of subsurface defects served as the initiation points of brittle-mode machining instead of surface crack formations. Under high external hydrostatic pressure, micro-crack propagation is arrested by the resultant compressive forces acting on these defects that arrest crack propagation as shown in Fig. 2a. However, surface cracks exposed to the high-pressure medium would add stresses at the crack tips and further promote surface crack propagation (Fig. 2b), which contradicts the experimental

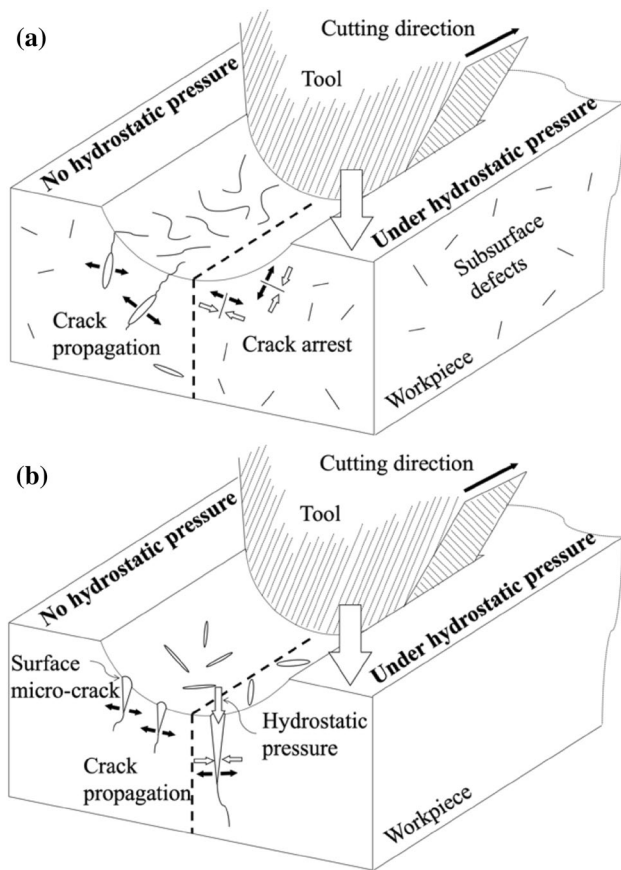


Fig. 2 Schematic of crack origins during machining under an externally applied hydrostatic pressure with (a) subsurface defects and (b) surface micro-cracks

findings of machining brittle materials under an external hydrostatic pressure.

The mechanism was further developed using an analytical model adapted from Griffith's theory on fracture mechanics. The fundamental criterion for crack elongation depends on the stress intensity factor induced by the stresses at the crack tip, which has to exceed the material fracture toughness for crack propagation. Yoshino et al. [17] explains that the resultant tensile stress acting on the subsurface defects is reduced by the hydrostatic pressure, which ultimately reduces the stress intensity factor.

While the benefits of enhancing the machinability of brittle materials under hydrostatic pressure are evident, sophisticated apparatuses are required to achieve the desirable machining benefits. In this work, surface solidified media will be applied on calcium fluoride (CaF_2) single crystals, as an easy means to induce an external compressive pressure that is analogous to the pressurized fluid acting on the workpiece during machining. In contrast to the current understanding of the hydrostatic pressures that generally suppress crack propagation on the machined surfaces, this work will

investigate the effects of the localized compressive pressure acting on the work material ahead of the cutting tool in the machining process. Ultraprecision orthogonal microcutting will be employed as a mature technique to first evaluate the effectiveness of the solidified layer in promoting ductile-mode machining at higher critical uncut chip thicknesses across different crystallographic orientations.

Chemical factors may also influence the ductility of brittle materials [13], and potentially affect the properties of the bulk material as a whole. Another class of reactions that may manifest, occurs through a chemisorption phenomenon. Recently, Chaudhari et al. [18] reported the alteration of material surface mechanical properties with the use of DYKEM permanent marker ink on copper and aluminum alloys during microcutting. They observed a reduction in cutting forces with thinner chip formation and attributed the phenomenon to the embrittlement of the chips under the temporary change in surface energy of the metallic surfaces. Westwood and Goldheim [19] reported the occurrence of similar surface-media effects on CaF_2 under active environments, explaining that the mobility of near-surface dislocations is restricted due to the electron or hole transfers between the material point defects and the surface-active media. Hence, microcutting and microhardness indentation experiments will be performed to disambiguate the working mechanism from chemical effects.

In addition, the degree of subsurface damage (SSD) will be evaluated through transmission electron microscopic analysis of the micromachined grooves. This is particularly important due to the post-machining residual stresses that commonly lead to lattice misalignments and further defect formations in the subsurface regions. SSD is also a major concern for the machining of optical materials, which hinders optical transmissivity and also results in the evolution of further material damage in the form of laser irradiation absorbance [20].

2 Experiments

2.1 Microcutting Setup

Experiments were performed on a Toshiba ULG100 ultraprecision diamond turning machine as shown in Fig. 3. Rotary and Z-axis movement is performed through an air bearing spindle. The X- and Y- positioning of the cutting tool is driven by servomotors. Calcium fluoride (CaF_2) samples with the (111) oriented face were procured from Latech Scientific Supply Pte. Ltd. The samples were waxed onto an aluminum plate that was mounted onto the air bearing spindle by a vacuum chuck. A single crystal diamond tool with a nose radius of 0.8 mm was used for trimming and orthogonal microcutting experiments. Flat sample surfaces

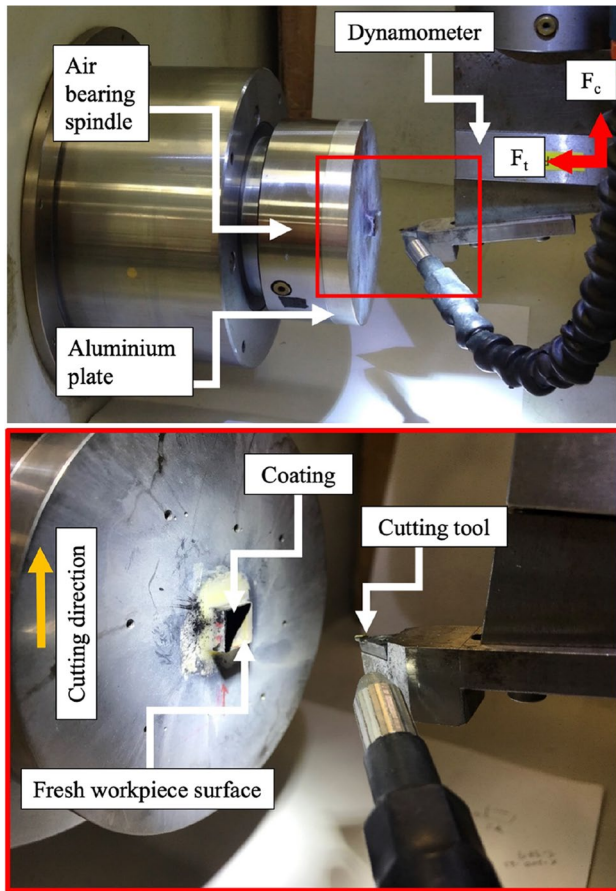


Fig. 3 Experimental setup on an ultraprecision machining centre

for precise alignment with the workpiece were produced by trimming for all experiments with cutting conditions stated in Table 1. The surface roughness of the prepared surfaces of CaF_2 was measured using an atomic force microscope (AFM) to be 2.07 nm Rq.

2.2 Progressive Microcutting

The crystallinity of both materials creates a challenging anisotropic behavior during machining, in that the critical uncut chip thickness varies with cutting direction. Lee et al. [21] performed crystal plasticity finite element method (CPFEM) simulation on a crystalline material and attributed the variation in cutting forces during face turning to the anisotropic

Table 1 CaF_2 trimming parameters

Machining parameter	Value
Spindle speed (rpm)	1200
Feed rate (mm/min)	1.2
Nominal depth of cut (μm)	2
Coolant	Oil mist

effects of the material. Hence, a series of progressive orthogonal microcutting experiments were performed along 15° intervals of the (111) workpiece surfaces as shown in Fig. 4 to analyze the anisotropic characteristics of the material. The diamond cutting tool was set with an effective rake angle of -10° and produced each groove at increasing depths at an inclination of 0.038° from 0 to $2 \mu\text{m}$ and a constant cutting speed of 50 mm/min. Dry cutting was selected to eliminate other factors that may influence the evaluation of the critical uncut chip thickness. Experiments were performed on unmodified surfaces of each material to serve as a reference for comparison. DYKEM high-purity 44 black ink [22] was applied as a coating and left to solidify on the workpiece surfaces for 30 min under normal air conditions, prior to the microcutting tests. For the tests with the coating, the tool path was defined to produce a microgroove with a final depth of $2 \mu\text{m}$ into the workpiece material.

The coat was subsequently removed by an ultrasonic bath in ethanol for 5 min for surface characterization. Optical microscopy and scanning electron microscopy (SEM) were employed to identify the DBT point, which is defined as the depth of cut where cracks appear on the surface. The respective critical uncut chip thicknesses of each groove can be calculated based on the defined tool geometry as shown in Fig. 4. Cutting forces (F_c) and thrust forces (F_t) were measured using a Kistler 9251B1 dynamometer and type 5051A amplifiers at a sampling rate of 10 kHz. Forces are analyzed at the DBT, which is determined by the transition from a smooth linear progression to an erratically fluctuating

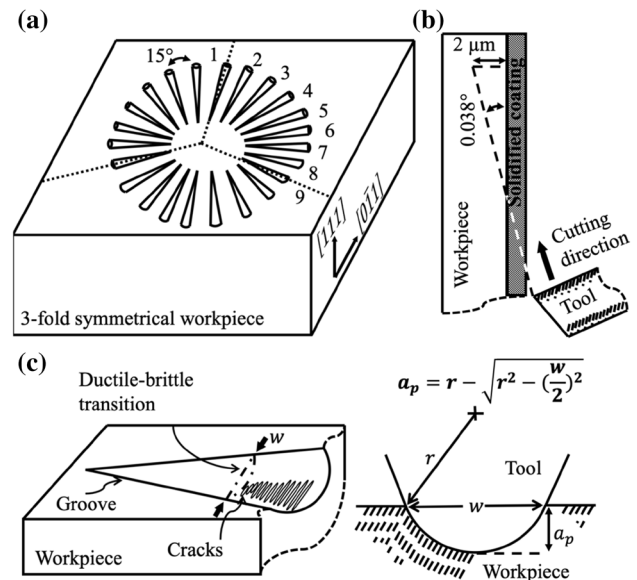


Fig. 4 Schematic of progressive orthogonal microcutting at 15° intervals: (a) top surface; (b) cross-section of a groove with solidified coating; (c) evaluation of critical uncut chip thickness based on tool geometry and the measured groove width, w

graph. While it is important to note that tool-tip vibration at the tool-workpiece and tool-chip interface may result in a similar fluctuation of forces [23, 24], the results observed in this work are mainly due to the energy dissipation from the formation of surface cracks [25]. Three sets of tests were performed to identify the average critical uncut chip thickness.

2.3 Verification of Mechanical Effect

The nature of interaction between the workpiece material and the applied coating was studied over three groups of indentation experiments that were performed using a Shimadzu HVM-2 micro Vickers hardness test machine. To verify changes in the mechanical properties due to potential chemical reactions on the surface, three sets of indentations were performed on the crystal at a constant load of 0.5 N and a dwelling time of 15 s. Three indentations were conducted to determine the average hardness for each case. Firstly, indentations on an unmodified surface were performed as a reference. Another set of indentations was carried out after applying a layer of ink that was left to dry under normal air conditions for 30 min and the last set of indentations was performed after removing the coating from the material surfaces. Indentation measurements were performed only after removal of the coating for each set of results to ensure fair comparison without the visual hindrance of the coating.

In addition, microgrooves of 500-nm constant depth (above the conventional critical uncut chip thickness) were produced by orthogonal microcutting on a face-turned CaF_2 sample along the $(111)[0\bar{1}1]$ direction at a cutting speed of 50 mm/min using the Toshiba ULG100 ultra-precision diamond turning machine. Prior to the grooving tests, the work piece was coated with a thin layer and left to dry for 30 min before subsequently applying another thicker layer on half the sample, such that the work material will be removed under a thin layer of coating and a subsequently thicker layer along the same groove.

2.4 Evaluation of Subsurface Damage

Orthogonal microgrooves were performed along the $(111)[0\bar{1}1]$ direction with a constant uncut chip thickness (300 nm—below the conventional critical uncut chip thickness) at 50 mm/min on the Toshiba ULG100 ultra-precision diamond turning machine to evaluate the effects of the solidified coating on the SSD. Half of the (111) sample surface was coated with layer of solidified coating, such that the groove will consist of regions with and without the influence of the solidified coating. Transmission electron microscopic (TEM) samples were prepared by a Helios 600i FEI focused ion beam (FIB) using the lift-out technique at crack-free locations on the groove. A layer of platinum (Pt) was first

applied on the nonconductive sample surface to aid image focusing on the scanning electron microscope (SEM), followed by a thicker layer of Pt deposited for ion beam protection during the ion milling process.

3 Results and Discussion

3.1 Progressive Microcutting

Following our previous work on CaF_2 in view of the 3-fold symmetry characteristic [26], 8 out of the 24 cutting directions (labelled as groove 1–9) will be presented for simplicity with the first groove oriented along the $[0\bar{1}1]$ direction. The minor differences in critical uncut chip thickness results from the references [26, 27] can be attributed to the difference in machine tool performance and tool geometries. Figure 5 presents the critical uncut chip thickness and the respective cutting and thrust forces along all cutting directions in a third of the sample surface. Figure 6 shows the distinct improvement in the DBT under the influence of the coating. The critical undeformed chip thickness values range from 9–447 nm under normal circumstances and a general improvement in critical uncut chip thickness is seen with the use of the solidified coating. Both cutting and thrust forces are seen to increase with the application of the solidified coating, which is a result of the additional material removal of the solidified coating. The threefold anisotropic characteristic of the (111) plane on CaF_2 are still preserved under the influence of the solidified coating.

3.2 Verification of Mechanical Effect

However, the increase in machining forces and inconsistent improvement in machinability with the solidified coating questions the working mechanism of the applied coating (i.e. chemical or mechanical). Any chemical interaction between a surface-active media and the workpiece should result in the temporary modification of surface mechanical properties and reflect as a constant enhancement in machinability, which was not observed in these set of results. Negligible differences in the material hardness of CaF_2 were observed prior to the application of the coating and after its removal as shown in Fig. 7. This indicates insignificant chemical affinity between the work material and the coating. A minor increase in the hardness during the indentation experiments with the solidified coating could be attributed to the resistance to deformation of the coating. This result presents further benefits to the machining process of these brittle materials, in that the mechanical integrity of the bulk material will not be altered by adopting this technique in precision machining. Figure 8 also confirms the absence of surface chemical

Fig. 5 Variation in ductile–brittle transition of the (111) CaF₂ with and without the application of solidified coating

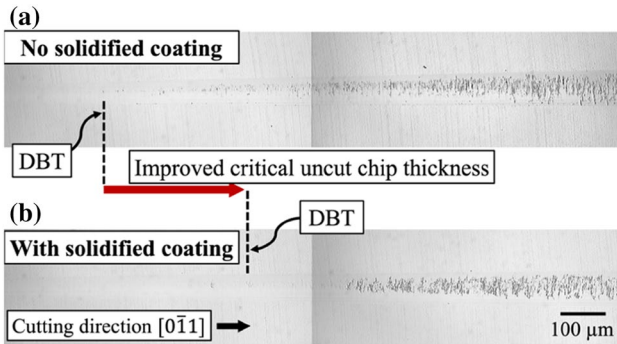
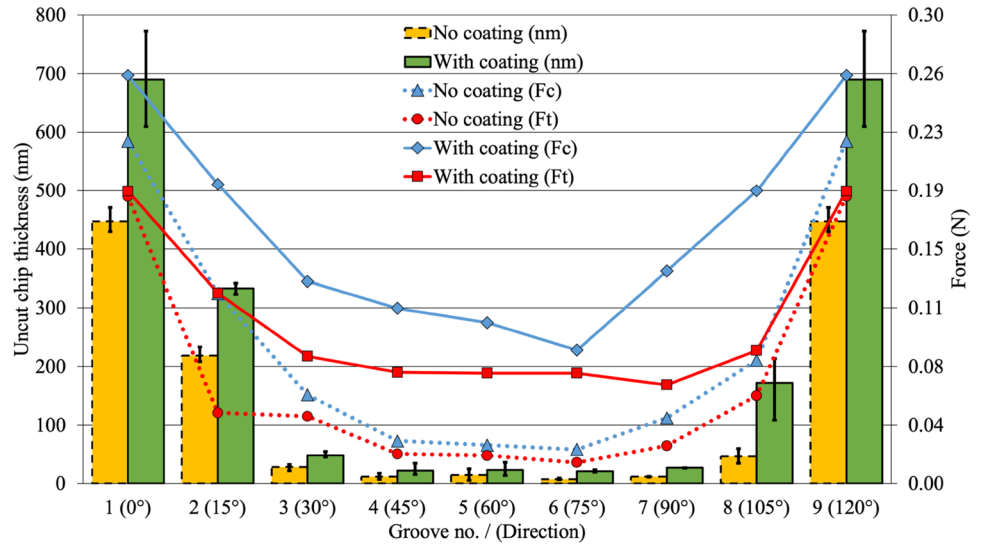


Fig. 6 Optical images of progressive orthogonal microgrooves on CaF₂ (a) without and (b) with the application of the solidified coating

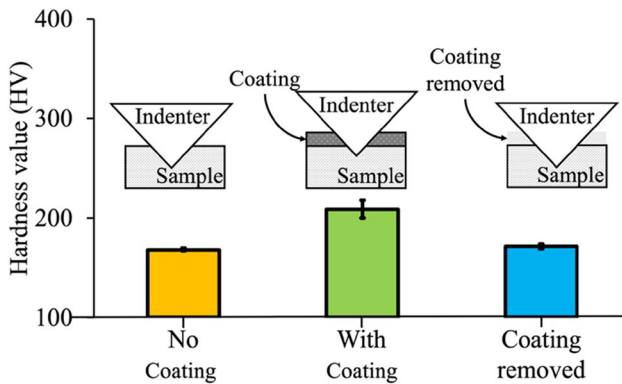


Fig. 7 Vickers microhardness of CaF₂ at a constant load of 0.5 N before applying the solidified coating, with the coating applied and after removing the coating

effects by exhibiting brittle-mode machining, even under the influence of the applied coating. Interestingly, the

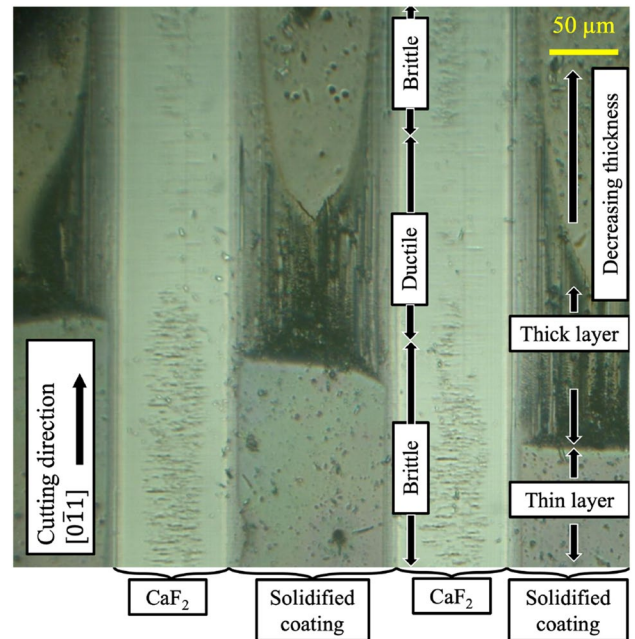


Fig. 8 Optical image of microgrooves produced with constant uncut chip thickness (500 nm) on CaF₂ along the (111) [011] direction with applied coating exhibiting ductile-mode and brittle-mode machining

ductile-regime still appears along the groove at the locations with evidently thicker layers of the coating. Correspondingly, as the coating thickness decreases along the groove, brittle cracks begin to resurface at a coating thickness of approximately 2.6 μm. The coating thickness may be measured based on the groove width in relation to the tool geometry in Fig. 4c. This implies that the machinability of these brittle materials is strongly dependent on mechanical influences of the solidified coating.

3.3 Evaluation of Subsurface Damage

The XTEM images of the samples shown in Figs. 9a and 10a display the SSD layer, which is described as a high-density dislocation zone in the immediate subsurface region [25]. The degree of damage can be analyzed through the different subsurface layers describing the crystal lattice arrangement. Blurred regions beneath the machined surface are determined to be the subsurface damaged layer induced during the microcutting process and measure up to 73 nm thick for the sample machined without applying the solidified coating as shown in Fig. 9a. The SSD layer is observed to be

reduced by ~45% to a thickness of 40 nm when machining with the solidified coating in Fig. 10a. A greater SSD layer is generally undesirable even though the top sample surface appears to be crack-free.

Fast Fourier transform (FFT) analyses in Figs. 9c and 10c are used to describe the crystallinity of the subsurface regions such that a highly damaged region would reveal a highly distorted diffraction pattern. The first region of analysis at Point 1 that is located immediately beneath the machined surface in both TEM samples show highly irregular lattice sites, which is associated with the highly damaged subsurface regions. Points 2 and 3 located further beneath

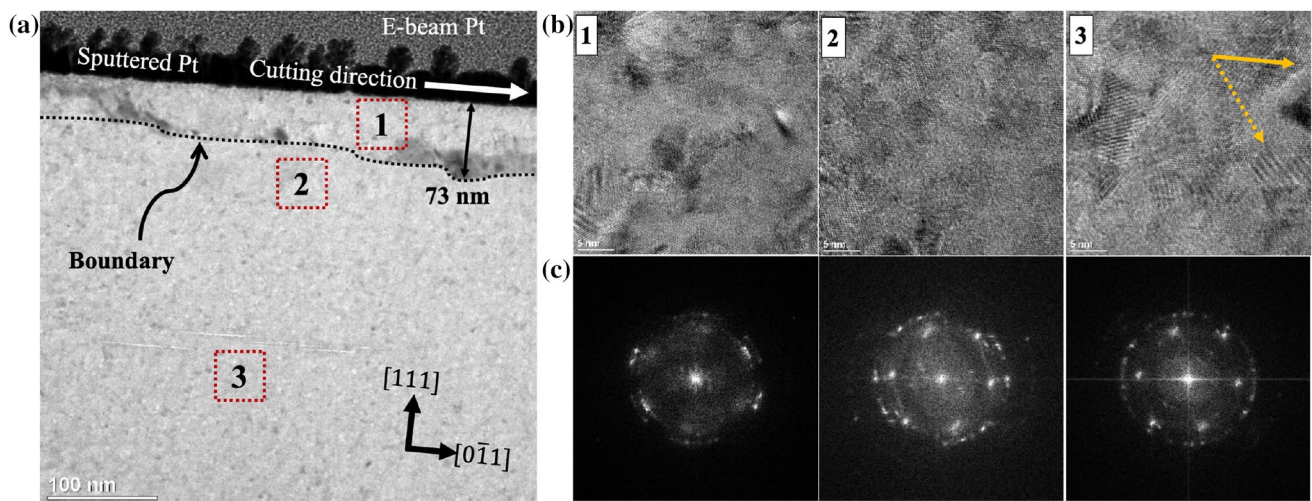


Fig. 9 Transmission electron microscopy (TEM) of CaF_2 machined subsurface without coating: (a) cross-sectional TEM (XTEM) overview of subsurface damage, (b) high resolution TEM (HRTEM) images of different regions and (c) the respective fast Fourier transform (FFT) analyses

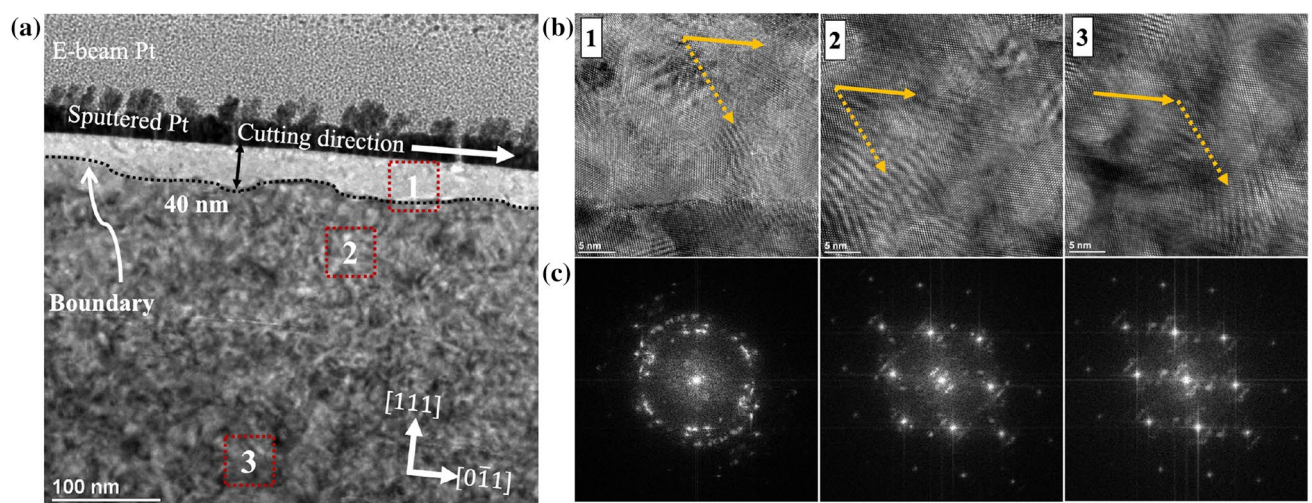


Fig. 10 Transmission electron microscopy (TEM) of CaF_2 machined subsurface with solidified coating: (a) cross-sectional TEM (XTEM) overview of subsurface damage, (b) high resolution TEM (HRTEM)

images of different regions and (c) the respective fast Fourier transform (FFT) analyses

the machined surface show the gradual restoration of the material crystallinity, which are determined as the transition zone where the degree of lattice deformation decreases gradually from the machined surface into the bulk material. The HR-TEM images at Points 2 and 3 of the sample prepared with the solidified coating in Fig. 10b show the slip deformation of atoms along the $(100)[0\bar{1}\bar{1}]$ slip system (indicated by the dotted arrow lines), which is the closest slip system angled at 54.7° from the (111) top surface (indicated by the solid arrow line) [28]. The FFT images in Fig. 10b confirm that the slip deformation is highly probable with the preservation of the material crystallinity. Contrarily, only a small hint of slip deformation can be observed in the HR-TEM image of the Point 3 of the sample prepared without the solidified coating in Fig. 9b. The FFT images in Fig. 9c further affirm the poor crystallinity of the areas of analysis, which could be attributed to a larger degree of rotational deformation in comparison to slip deformation. Wang et al. [26] also reported the occurrence of lattice rotation in the machined subsurface layer in microcutting of CaF_2 along the $(111)[0\bar{1}\bar{1}]$ direction. The evidence of slip deformation occurring under the influence of the solidified coating potentially leads to shallower SSD layers [29].

Figure 11 shows the cutting forces measured for the 300-nm microgroove prepared along the $(111)[0\bar{1}\bar{1}]$ direction for TEM analysis. The initial dominance of thrust forces to cutting forces at the start of the groove is a result of tool-edge-radius size effects [30] occurring as the tool gradually enters the work material and should not be considered in this analysis. The angles of the resultant forces with and without the influence of the solidified coating show negligible differences, averaging at approximately 48° to the normal of

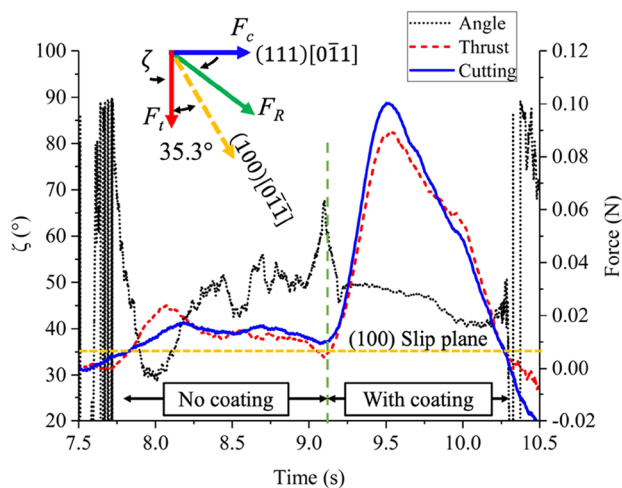


Fig. 11 Measured forces during microcutting of a 300-nm groove along $(111)[0\bar{1}\bar{1}]$ in CaF_2 from a region with no coating to a region with coating and the respective angles of the resultant force into the workpiece

the machined surface. This indicates that the angles of the resultant force acting into the work material in relation to the (111) cleavage and (100) slip planes of CaF_2 , are similar for both surface conditions. Mizumoto et al. [25] described the subsurface distortion of the lattice arrangement as a result of shear deformation and rotation deformation followed by elastic recovery to form the finished surface. The 12.7° difference between the resultant force direction and the $(100)[0\bar{1}\bar{1}]$ slip system as shown in Fig. 11 results in both rotation and slip deformation of the immediate subsurface lattices for both cases as observed from the SSD analyses in Figs. 9a and 10a.

However, it is evident that the resultant force angle is in a far more stable state under the influence of the coating than the angles observed without. This highly unstable change in resultant force directions potentially changes the deformation and slip processes in the subsurface lattice regions, which explains the observation of the highly disordered subsurface shown in the HR-TEM and FFT images of Fig. 9b and c. It appears that the resistance to deformation of the solidified coating controls the direction of the resultant machining forces by inducing reactive compressive stresses into the work material to enable a stable slip deformation process of the subsurface regions and reduces the degree of subsurface lattice rotation.

In addition, cutting chips can be observed as shown in Fig. 12a, which is likely to compose of the ink-coating given the size and thickness of the chip relative to the actual cutting depth of 300 nm into CaF_2 . It is important to note that the observation of CaF_2 chips in this process is extremely difficult due to the thickness differences between the coating and the uncut chip thickness, as well as the colorless nature of CaF_2 in comparison to the black coating. However, the formation of a chip displaying minor serrations similar to those observed in metal cutting suggests that the solidified coating adhered to the work material surface during the material removal process and effectively provided the compressive stresses on the work material due to its resistance to deformation.

During the conventional CaF_2 chip formation process, shear strain of different magnitudes occurs on multiple activated slip systems in the primary deformation zone within the chip [26]. This potentially causes the formation of an irregularly shaped chip that influences the forces on the tool-chip interface, which consequently affects the resultant force inclination angle (ζ) shown in Fig. 11. On the contrary, the adhered coating and the cutting tool will sandwich the CaF_2 chip as described in Fig. 12b to control the shearing action and enable a stable chip formation process. The relatively consistent inclination angle of the resultant force (F_R) in Fig. 11 indicates a stable resolved shear angle in the primary deformation zone. As such, the chip formation process under the influence of the solidified

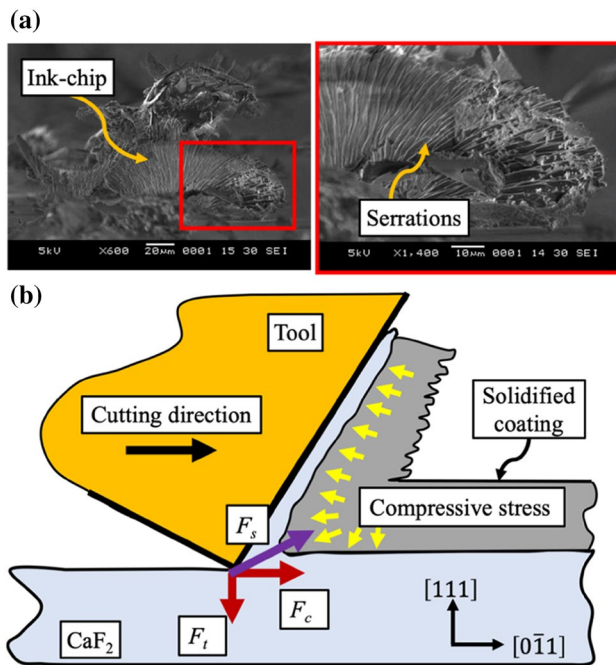


Fig. 12 **a** Chip morphology of the solidified coating and **(b)** a schematic of the compressive stresses acting on the work material and chip formation during orthogonal cutting

coating will inevitably undergo a well-controlled process. Uezakk et al. [31] also observed similar smoothing of the chip formation process through molecular dynamics simulation of a hydrostatic pressure induced by a jig ahead of the cutting tool.

Therefore, the working mechanism in this paper differs from the understanding of previous works under an ambient hydrostatic pressure that focused on the suppression of crack propagation on the machined surfaces. Instead, the compressive stresses here are locally induced ahead of the cutting tool to enable a steady cutting process. The compressive stress should intuitively occur during cutting in a pressurized chamber by simply substituting the solidified coating with the pressurized fluids, such that the fluid will induce an external compressive pressure onto the work material and the produced chip.

4 Conclusions

Following the successful improvements in machinability under high hydrostatic pressure, a similar effect can be observed by machining brittle materials coated with solidified coating. (111) oriented single crystal calcium fluoride was tested by microindentation and orthogonal microcutting experiments to arrive at the following conclusions:

1. Application of solidified coating (minimally $\sim 2.6 \mu\text{m}$ thick for DYKEM permanent marker ink) on the pre-machined workpiece surface significantly increases the critical uncut chip thickness along different cutting directions of the (111) CaF_2 single crystal;
2. Microcutting with the solidified coating has no impact on the anisotropic properties;
3. Potential chemical influences on the workpiece surfaces are also deemed insignificant in comparison to the mechanical influence by the solidified layer;
4. A significant reduction in subsurface lattice misalignment is observed by $\sim 45\%$ in orthogonal microcutting of CaF_2 with the solidified coating; and
5. The reduced subsurface damage is a result of the relatively constant resultant machining force direction acting into the work material, which enables a stable subsurface slip deformation process under the influence of the solidified coating.

The implementation of this developed technique can potentially reduce the need for coolant to achieve higher material removal rates in micromachining and thus reduce the pollution of microfluids released into the machining environment [2], satisfying the several considerations for green manufacturing as described by Dornfeld [32]. Moreover, reduced subsurface damages would significantly shorten the time required on the post-processing of optical components [33]. For instance, one can no longer rely on the secondary polishing process using large quantities of abrasive slurries that are rarely recycled to incrementally remove the damaged layer to produce high quality optical products.

Acknowledgements The authors express their gratitude to Mr. Yeo Eng Huat, Nelson (AML, NUS) for his assistance in performing the experiments. The financial supports from the National University of Singapore Start-up Grant (Grant No.: R-265-000-564-133), Singapore Ministry of Education Academic Research Fund Tier 1 (Grant No.: R-265-000-593-114), and AcRF Tier 2 Funding (Project No: MOE2018-T2-1-140) are sincerely appreciated.

Compliance with Ethical Standards

Conflict of interest On behalf of all authors, the corresponding author states that there is no conflict of interest.

References

1. Yan, J., Syoji, K., & Kuriyagawa, T. (2000). Diamond turning of CaF_2 for nanometric surface. *American Society for Precision Engineering Proceedings*, 22, 66–69.
2. Schneider, F., Das, J., Kirsch, B., Linke, B., & Aurich, J. C. (2019). Sustainability in ultraprecision and micro machining: a review. *International Journal of Precision Engineering and Manufacturing-Green Technology*. <https://doi.org/10.1007/s40684-019-00035-2>.

3. Lee, Y. J., Chaudhari, A., Zhang, J., & Wang, H. (2019). Thermally assisted microcutting of calcium fluoride single crystals. In J. Zhang, B. Guo, & J. Zhang (Eds.), *Simulation and experiments of material-oriented ultra-precision machining* (pp. 77–127). Singapore: Springer.
4. Antwi, E. K., Liu, K., & Wang, H. (2018). A review on ductile mode cutting of brittle materials. *Frontiers of Mechanical Engineering*, 13, 251–263.
5. Nakasuji, T., Kodera, S., Hara, S., & Ikawa, N. (1990). Diamond turning of brittle materials for optical components. *CIRP Annals—Manufacturing Technology*, 39, 89–92.
6. Suzuki, N., Nakamura, A., Shamoto, E., Hara, K., Matsuo, M., & Osada, M. (2004). Ultraprecision micromachining of brittle materials by applying ultrasonic elliptical vibration cutting. In *Micro-Nanomechanics and Human Science, 2004 and The Fourth Symposium Micro-Nanomechanics for Information-Based Society*, 2004 (pp. 113–38).
7. To, S., Wang, H., & Jelenković, E. V. (2013). Enhancement of the machinability of silicon by hydrogen ion implantation for ultra-precision micro-cutting. *International Journal of Machine Tools and Manufacture*, 74, 50–55.
8. Wang, H., Kumar, A. S., & Riemer, O. (2018). On the theoretical foundation for the microcutting of calcium fluoride single crystals at elevated temperatures. *Proceedings of the Institution of Mechanical Engineers, Part B*, 232, 1123–1129.
9. Chaudhari, A., Lee, Y.J., Wang, H. & Kumar, A.S. (2017). Thermal effect on brittle-ductile transition in CaF₂ single crystals. In *Proceedings of the 17th international conference of the european society for precision engineering and nanotechnology, EUSPEN 2017*.
10. Jeon, Y., & Lee, C. M. (2012). Current research trend on laser assisted machining. *International Journal of Precision Engineering and Manufacturing*, 13, 311–317.
11. Yoshino, M., Aoki, T., Sugishima, T., & Shirakashi, T. (1999). Scratching test on hard-brittle materials under high hydrostatic pressure. *Seimitsu Kogaku Kaishi/ Journal of Japan Society for Precision Engineering*, 65, 1481–1485.
12. Yan, J., Yoshino, M., Kurigawa, T., Shirakashi, T., Syoji, K., & Komanduri, R. (2001). On the ductile machining of silicon for micro electro-mechanical systems (MEMS), opto-electronic and optical applications. *Material Science and Engineering A*, 297, 230–234.
13. Bridgman, P. W. (1947). The effect of hydrostatic pressure on the fracture of brittle substances. *Journal of Applied Physics*, 18(2), 246–258.
14. Kaitkay, P., & Lei, S. (2004). Experimental study of rock cutting under external hydrostatic pressure. *Journal of Materials Processing Technology*, 159(2), 206–213.
15. Sreejith, P. S., & Ngoi, B. K. A. (2001). Material removal mechanisms in precision machining of new materials. *International Journal of Machine Tools and Manufacture*, 41(12), 1831–1843.
16. Yoshino, M., Aoki, T., Shirakashi, T., & Komanduri, R. (2001). Some experiments on the scratching of silicon : in situ scratching inside an SEM and scratching under high external hydrostatic pressures. *International Journal of Mechanical Sciences*, 43, 335–347.
17. Yoshino, M., Ogawa, Y., & Aravindan, S. (2005). Machining of hard-brittle materials by a single point tool under external hydrostatic pressure. *Journal of Material Science and Engineering*, 127(7), 837–845.
18. Chaudhari, A., Soh, Z. Y., Wang, H., & Kumar, A. S. (2018). Rebinder effect in ultraprecision machining of ductile materials. *International Journal of Machine Tools and Manufacture*, 133, 47–60.
19. Westwood, A. R. C., & Goldheim, D. L. (1968). Occurrence and mechanism of rebinder effects in CaF₂. *Journal of Applied Physics*, 39, 3401–3405.
20. Trost, M., Herffurth, T., Schröder, S., Duparré, A., & Tünnermann, A. (2014). Evaluation of subsurface damage and surface roughness by light scattering techniques. *Applied Optics*, 52, 6579–6588.
21. Lee, W. B., Wang, H., Chan, C. Y., & To, S. (2013). Finite element modelling of shear angle and cutting force variation induced by material anisotropy in ultra-precision diamond turning. *International Journal of Machine Tools and Manufacture*, 75, 82–86.
22. ITW-PROBRANDS, Material safety data sheet-high purity 44 2016. https://itwprofessionalbrands.com/msds/169_0.pdf. Accessed Dec 2018.
23. Wang, H., To, S., Chan, C. Y., Cheung, C. F., & Lee, W. B. (2011). Dynamic modelling of shear band formation and tool-tip vibration in ultra-precision diamond turning. *International Journal of Machine Tools and Manufacture*, 51, 512–519.
24. Wang, H., To, S., & Chan, C. Y. (2013). Investigation on the influence of tool-tip vibration on surface roughness and its representative measurement in ultra-precision diamond turning. *International Journal of Machine Tools and Manufacture*, 69, 20–29.
25. Mizumoto, Y., Amano, H., Kangawa, H., Harano, K., Sumiya, H., & Kakinuma, Y. (2018). On the improvement of subsurface quality of CaF₂ single crystal machined by boron-doped nanopolycrystalline diamond tools. *Precision Engineering*, 52, 73–83.
26. Wang, H., Riemer, O., Rickens, K., & Brinksmeier, E. (2016). On the mechanism of asymmetric ductile-brittle transition in micro-cutting of (111) CaF₂ single crystals. *Scripta Materialia*, 114, 21–26.
27. Mizumoto, Y., & Kakinuma, Y. (2018). Revisit of the anisotropic deformation behavior in single-crystal CaF₂ in orthogonal cutting. *Precision Engineering*, 53, 9–16.
28. Azami, S., Kudo, H., Mizumoto, Y., Tanabe, T., Yan, J., & Kakinuma, Y. (2015). Experimental study of crystal anisotropy based on ultra-precision cylindrical turning of single-crystal calcium fluoride. *Precision Engineering*, 40, 172–181.
29. Mizumoto, Y., Kangawa, H., Itobe, H., Tanabe, T., & Kakinuma, Y. (2017). Influence of crystal anisotropy on subsurface damage in ultra-precision cylindrical turning of CaF₂. *Precision Engineering*, 49, 104–114.
30. Huo, D., & Cheng, K. (2013). Micro cutting mechanics. In K. Cheng & D. Huo (Eds.), *Micro-cutting: fundamentals and applications* (pp. 19–44). United Kingdom: Wiley.
31. Uezaki, K., Shimizu, J., & Zhou, L. (2014). Development of metal cutting process accompanied by a localized compressive hydrostatic stress field formation: examination by molecular dynamics simulation. *Precision Engineering*, 38(2), 371–378.
32. Dornfeld, D. A. (2014). Moving towards green and sustainable manufacturing. *International Journal of Precision Engineering and Manufacturing-Green Technology*, 1(1), 63–66.
33. Jiang, C., Wu, T., Ye, H., Cheng, J., & Hao, Y. (2019). Estimation of energy and time savings in optical glass manufacturing when using ultrasonic vibration-assisted grinding. *International Journal of Precision Engineering and Manufacturing-Green Technology*, 6, 1–9.

Publisher's Note Springer Nature remains neutral with regard to jurisdictional claims in published maps and institutional affiliations.



Mr. Yan Jin Lee is a PhD candidate at Department of Mechanical Engineering, National University of Singapore. His research interests include machining of brittle materials and mechanochemical effects in ultra-precision machining.



Dr. Akshay Chaudhari is Research Fellow at Department of Mechanical Engineering, National University of Singapore. His research interests include ultra-precision machining, sustainable metal working fluids, deep hole drilling and additive manufacturing.



Ms. Jing Yi Chong is a final-year BEng student at Department of Mechanical Engineering, National University of Singapore. Her research interests include ultra-precision machining and mechanical behaviours of single crystals.



Dr. Hao Wang is Alexander von Humboldt Fellow and Assistant Professor at Department of Mechanical Engineering, National University of Singapore. His research interests include ultra-precision machining and hybrid manufacturing technologies, material-oriented micro-/nano-cutting mechanisms, and multiscale modelling and simulation.